Magnetic fabric and sedimentary characterization of near-slope to basinal deposits from the Chicontepec Formation, central and southern region of the Tampico-Misantla basin

Fábrica magnética y caracterización de depósitos sedimentarios cercanos a la cuenca de la Formación Chicontepec, región centro y sur de la cuenca Tampico-Misantla

Roberto Stanley **Molina-Garza**[1,†], María Isabel **Sierra-Rojas**[2,*]

[1] Centro de Geociencias, Universidad Nacional Autónoma de México, Blvd. Juriquilla 3001, Querétaro, México.

[2] Departamento de Geociencias, Universidad de los Andes, Cra 1 # 18a-12, Bogotá D.C., Colombia.

[†] En memoria de su trabajo.

* Corresponding author: (M. I. Sierra-Rojas) *isabelsr@geologia.unam.mx*

How to cite this article:
Molina-Garza, R., Sierra-Rojas, M., 2022, Magnetic fabric and sedimentary characterization of near-slope to basinal deposits from the Chicontepec Formation, central and southern region of the Tampico-Misantla basin: Boletín de la Sociedad Geológica Mexicana, 74 (1), A161021. http://dx.doi.org/10.18268/BSGM2022v74n1a161021

Manuscript received: August 23, 2021
Corrected manuscript received: September 30, 2021
Manuscript accepted: October 17, 2021

Peer Reviewing under the responsibility of Universidad Nacional Autónoma de México.

ABSTRACT

We report results of a study of the Chicontepec Formation magnetic fabric in the central and southern region of the Tampico-Misantla basin in the state border region between Veracruz and Hidalgo. Samples were collected at 16 sites corresponding to two main facies associations: channel-fill facies and channel overbank facies. The channel facies dominate the relief developing prominent geoforms adjacent to low hills developed in facies dominated by shales. Measurements were made on channel and overbank facies. Laboratory analyses include anisotropy of magnetic susceptibility (AMS) and remanence anisotropy (AARM), as well as isothermal remanence acquisition (IRM) and thermomagnetic curves to characterize magnetic mineralogy. The magnetic susceptibility values of the entire collection are of the order of 40 to 70 x10^{-6} SI, so the susceptibility fabric is controlled by the paramagnetic fraction. The IRM acquisition curves are near saturation with inductions < 0.3 T and can be modeled with a low coercivity component contributing ~ 90% and a high coercivity component contributing < 10%. The thermomagnetic curves are dominated by paramagnetic phases. In the AMS fabric, three types of behavior are observed, corresponding to a lesser extent to sedimentary fabrics (k3 ~ vertical), and mostly to incipient and well-developed tectonic fabrics. The sedimentary fabrics are characterized by the imbrication of the magnetic foliation perpendicular to the paleocurrent data obtained in the field, which are generally consistent from NW to SE. At sites with tectonic fabric, which generally correspond to sites closer to the deformation front, the magnetic lineaments are well clustered in the NW quadrant with low plunges. AMS and AARM fabrics may combine in complex patterns. AARM appears to record either maximum axis directions that correspond to alignment of elongated particles perpendicular to flow or the direction of thrust motion.

Key words: magnetic fabric, Chicontepec Formation, turbidite systems.

RESUMEN

Presentamos los resultados de un estudio de la fábrica magnética de la Formación Chicontepec en la región central y sur de la cuenca Tampico-Misantla cerca del límite estatal entre Veracruz e Hidalgo. Se recolectaron muestras en 16 sitios correspondientes a dos asociaciones de facies principales: facies de relleno de canal y facies de desborde de canal. Las facies del canal dominan el relieve desarrollando geoformas prominentes adyacentes a colinas bajas desarrolladas en facies dominadas por lutitas. Se realizaron mediciones en facies de canal y de desborde de canal. Los análisis de laboratorio incluyen anisotropía de susceptibilidad magnética (AMS) y anisotropía de remanencia (AARM), así como adquisición de remanencia isotérmica (IRM) y curvas termomagnéticas para caracterizar la mineralogía magnética. Los valores de susceptibilidad magnética son del orden de 40 a 70 x 10^{-6} SI, por lo que la fábrica de susceptibilidad está controlada por la fracción paramagnética. Las curvas de adquisición de IRM están cerca de la saturación con inducciones < 0.3 T y se pueden modelar con un componente de baja coercitividad que contribuye con ~ 90% y un componente de alta coercitividad que contribuye con < 10%. Las curvas termomagnéticas están dominadas por fases paramagnéticas. En la fábrica AMS se observan tres tipos de comportamiento, correspondientes en menor medida a fábricas sedimentarias (k3 ~ vertical), y sobre todo a fábricas tectónicas que van de incipientes a bien desarrolladas. Las fábricas tectónicas se caracterizan por la imbricación de la foliación magnética perpendicular a los datos de paleocorriente obtenidos en campo, que generalmente son consistentes de NW a SE. Los sitios con fábrica tectónica generalmente corresponden a sitios cercanos al frente de deformación o de niveles estructurales profundos. Las lineaciones magnéticas de varios sitios están bien agrupadas en el cuadrante SW en la dirección de movimiento en las cabalgaduras.

Palabras clave: fábrica magnética, Formación Chicontepec, sistemas turbidíticos.

http://dx.doi.org/10.18268/BSGM2022v74n1a161021

1. Introduction

The Tampico-Misantla basin, in the coastal plain of the Gulf of Mexico in eastern Mexico, is a Paleogene foreland basin associated with the Sierra Madre Oriental (SMO) fold and thrust belt. The Upper Cretaceous and Lower Paleocene is a hiatus that has been interpreted as the result of erosion of unconsolidated sediment that formed a network of interconnected canyons that in Mexican literature is referred to as the Chicontepec paleo-channel (Busch and Amado, 1978; Cossey *et al.*, 2019). The canyons were in turn filled by ~ 2000 meters of siliciclastic strata of the Chicontepec Formation.

Chicontepec is described as an upper Paleocene -lower Eocene rhythmic alternation of sandstone, shale, and mass transport complexes interpreted as a syntectonic deep-water siliciclastic turbidite system (Santillán-Piña and Camargo, 2011). It is of high economic interest because of the presence of non-conventional hydrocarbon resources and well-established conventional oil fields. The main source of detritus to the Chicontepec system is emergent land in the SMO fold belt to the west and NW (González-Díaz *et al.*, 2018), and perhaps sources in the Tuxpan platform to the east. Deformation of the SMO continued during deposition of the Chicontepec Formation, which is folded along the foldbelt front. Deformation, however, occurred at shallow structural levels as there is no cleavage development during folding. We studied the magnetic fabric of the Chicontepec Formation in the southern part of the canyon system, between Chicontepec and Venustiano Carranza (Figure 1) in the SW part of the basin, in order to evaluate the preservation of paleo-current information in sandstone channels and channel overflow facies.

The magnetic anisotropy of rocks results from preferential alignment of crystallographic or particle axes and the intrinsic anisotropy of mineral phases. Anisotropy defines a magnetic fabric approximated by a tri-dimensional ellipsoid, with maximum, intermediate, and minimum axes corresponding to the principal directions of a symmetric second order tensor that relates the applied magnetic field and the induced magnetization (anisotropy of magnetic susceptibility or AMS). The "magnetic foliation" is defined by the maximum and intermediate axes, and in sedimentary rocks is often imbricated in the upstream direction against the bedding plane by the effect of currents on flattened grains. It has also been reported that magnetic lineation (the maximum axis of the ellipsoid) may be aligned with paleocurrent direction in the case of elongated grains, or be perpendicular to it in high flow regimes. The cause of these relations has been theoretically and experimentally analyzed (Rees and Woodall, 1975; Hrouda, 1982; Borradaile *et al.*, 1999), but the actual mechanisms that cause preferential particle alignment in nature and the hydrodynamic behavior of sediment particles are difficult to reproduce and model.

The magnetic anisotropy observed is, however, the superposition of fabrics of different origin and orientation. It has been recognized that burial and compaction increase magnetic anisotropy (Imaz *et al.*, 2000). It has also long been recognized that the magnetic fabric of fine-grained sedimentary rocks evolves as deformation progresses (Graham, 1966; Parés *et al.*, 1999; Robion *et al.*, 2007), passing from a sedimentary to a composite, to a tectonic fabric (Parés *et al.*, 1999), or described as type 1 (sedimentary), types 2 and 3 (intermediate), or types 4, 5 and 6 (tectonic) fabrics (Robion *et al.*, 2007. Sedimentary fabric generally preserves a near vertical minimum susceptibility axis and magnetic foliation may record paleo-current direction during deposition (Hamilton and Rees, 1970). Tectonic fabric is generally parallel to the principal stress tensor, with the maximum susceptibility axis perpendicular to the shortening direction (Hrouda, 1982; Borradaile, 1988; Robion *et al.*, 2007). We conclude that the Chicontepec Formation and overlying strata preserve primary sedimentary fabrics which have also been modified by progressive deformation, forming tectonic fabrics.

2. Local geology and sampling

The Chicontepec Formation crops out in the western and southern portions of the Tampico-Mis-

http://dx.doi.org/10.18268/BSGM2022v74n1a161021

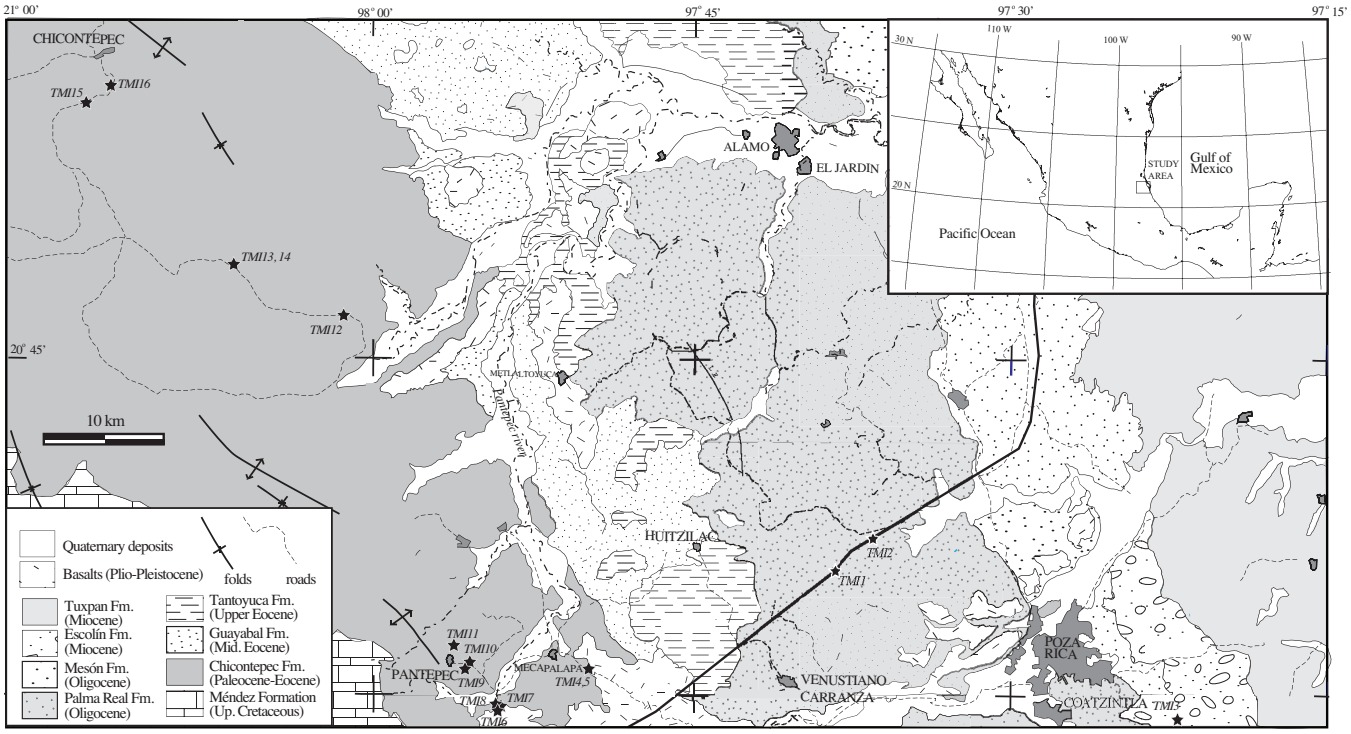

Figure 1 **Geologic map of the southern portion of the Tampico-Misantla basin (after Servicio Geológico Mexicano, 2004) with sampling sites (stars).**

antla basin, but it is also recognized by extensive drilling in the rest of the basin. Near the boundary between Hidalgo and Veracruz states in the Chicontepec paleo-canyon (Cossey. *et al* ., 2019), we identified three main facies associations: massive conglomerate facies (debrites), channel-fill facies, and channel overbank facies. The conglomeratic and channel facies form prominent geoforms with cliffs adjacent to smooth hills developed in shale dominated facies. Our study concentrated in channel-fill and channel overbank facies of the Chicontepec Formation (Figure 2). We also collected samples from two sites (TMI1 and 2) in the Palma Real turbidites of Oligocene age, and one site in the Escolín Formation (TMI3). Palma Real is an intercalation of light brown shale, massive, with lenticular sandstone bodies (channels). Palma Real along Highway 132D (Mexico-Tuxpan toll road) consists of channel systems with lateral-accretion that migrate to the NW. The section we sampled contains at the base massive debrites with rounded limestone clasts floating in a mudstone matrix underlying a rhythmic succession of sandstone (80 - 85%) and mudstone (Figure 3H). The succession shows thinning and fining upward trends in the sandstones, and it is interpreted as a system of wide channels with low sinuosity and sourced in the SW, based on flute casts.

Outcrops of the Chicontepec Formation near the Mecapalapa locality (sites TMI4 and 5; 20.52068N, - 97.83914W) are characterized by cyclic successions of fissile shale 10 to 15 cm thick and medium to fine sandstone in thin beds 3 to 7 cm thick (Figures 3A and 3B). The succession is dominated by mudstone, which becomes more abundant towards the top. Sandstone beds have erosive bases and commonly present current ripple laminations. These characteristics are typical of overbank deposits. In this region most paleocurrent indicators in overbank strata show flow from the SW (oblique to channel flow).

The succession is overlain by a section dominated by coarse to medium sandstones, with normal grading or massive in beds 50 to 70 cm thick

http://dx.doi.org/10.18268/BSGM2022v74n1a161021

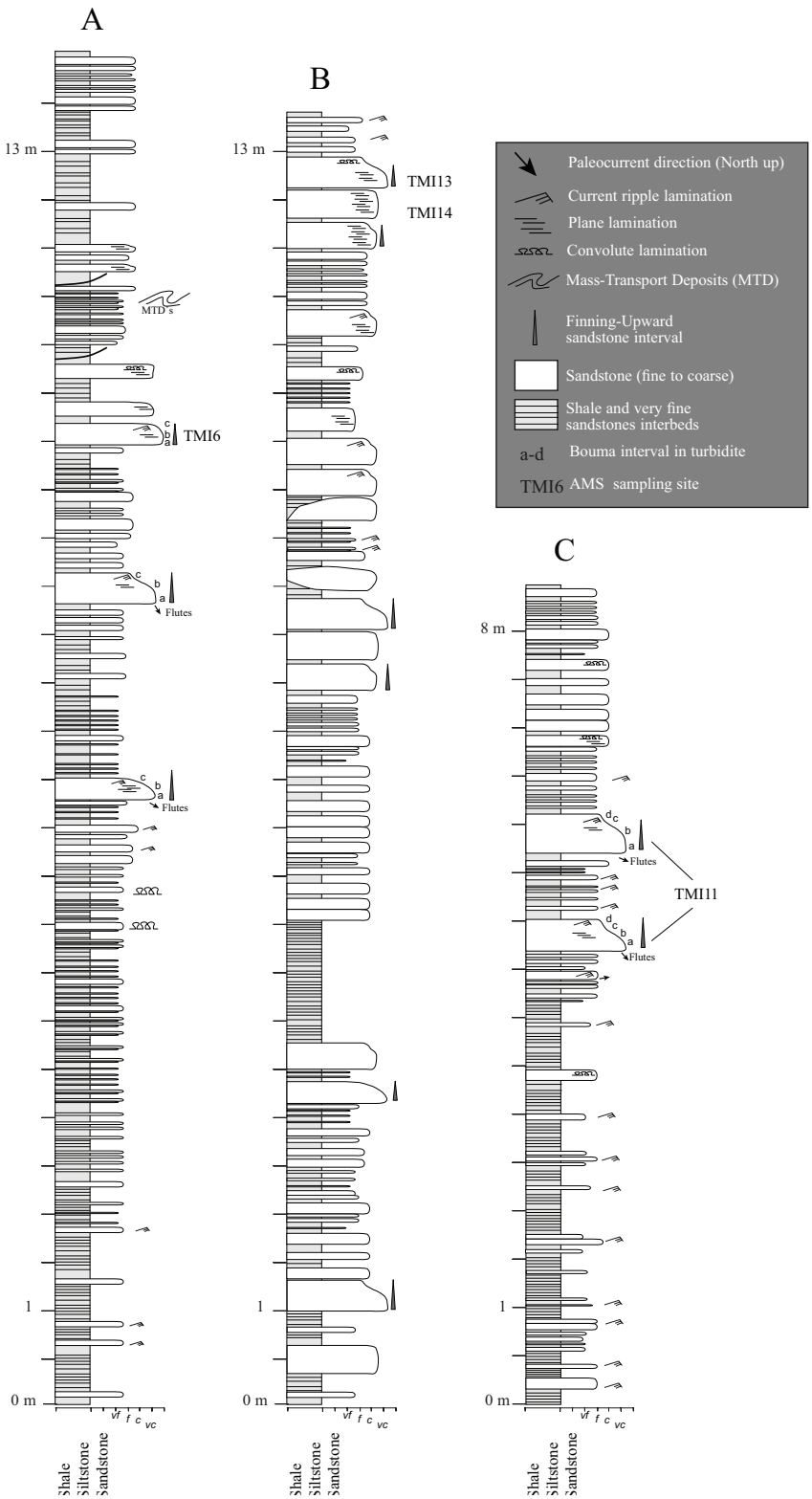

Figure 2 Measured stratigraphic sections of the Chicontepec Formation at: A) Road from Pantepec to Apapantilla, near Pantepec river (20.491817 ºN - 97.89687 ºW), B) Puente El Aguacate near Chicontepec, and C) along the road from Pantepec to Apipilhuaso (20.536657 ºN - 97.93102 ºW).Tampico-Misantla basin (after Servicio Geológico Mexicano, 2004) with sampling sites (stars).

http://dx.doi.org/10.18268/BSGM2022v74n1a161021

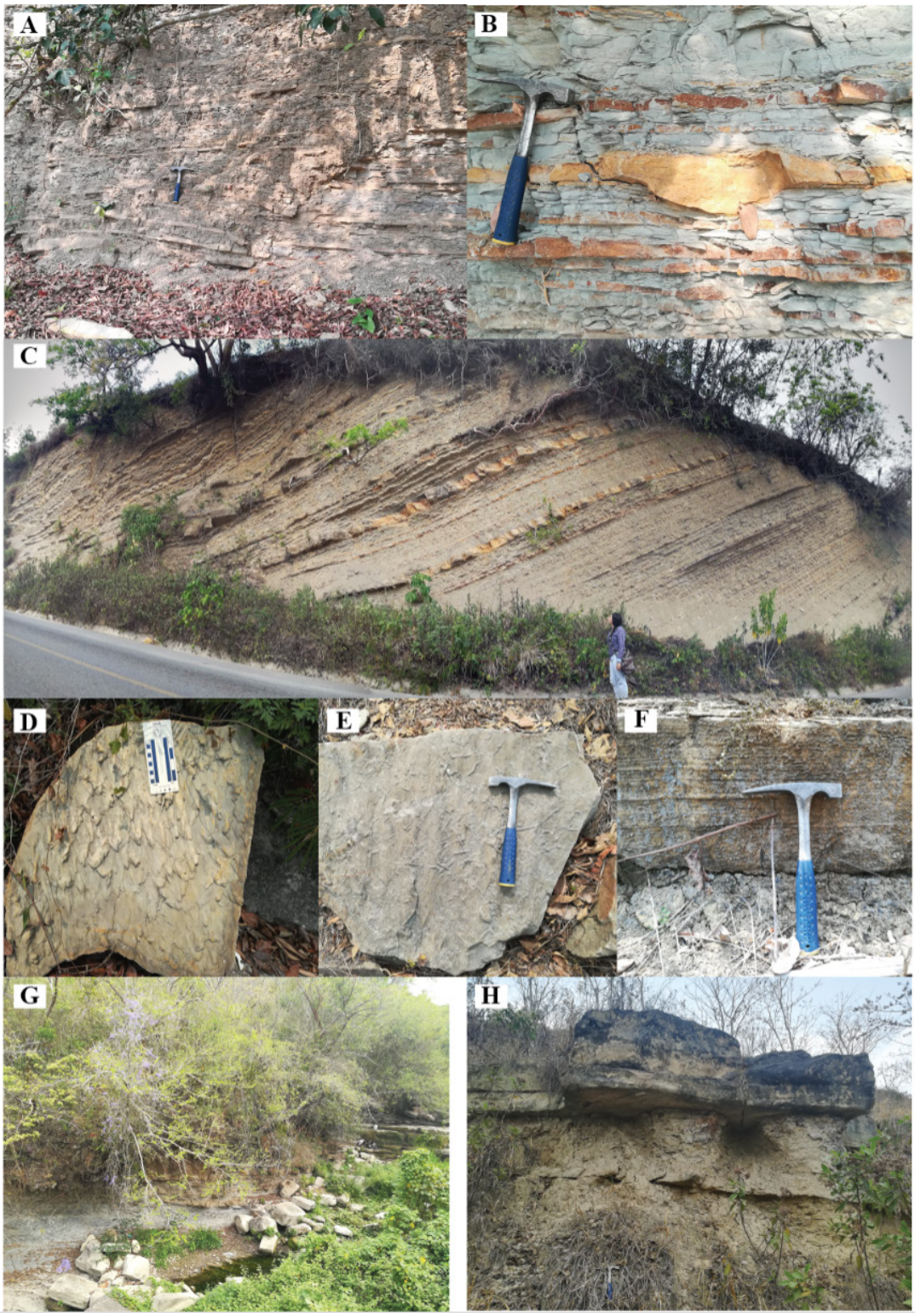

Figure 3 Representative photographs of the outcrops. A and B are intercalations of sandstone and mudstone beds, with common cut and fill structures corresponding to small, channelized flow (site TMI4). C- cyclic very fine sandstone and shale intercalations (right hand side of photograph), interrupted by beds of medium-grained sandstone (site TMI6 and 7; Mecapalapa area). D- flute casts, E- trace fossils, and F- laminated normally graded sandstone from the Pantepec area. Fig. 3G sites TMI13 and 14 in sandstone channels of the Chicontepec Formation. H- Sandstone channel in the Oligocene Palma Real Formation.sampling sites (stars).

and notable lateral continuity (Figures 2A and 3C, sites TMI6 and 7; 20.491817 ºN - 97.89687 ºW). These are intercalated with shale and very fine sandstone beds that contain plane lamination and flute casts, in beds 5 to 15 cm thick. We observed ample lens-shaped sandstone bodies of coarse- to fine-sandstone 25 to 50 cm thick with normal grading, planar laminations, and in some cases ripples corresponding to Ta to Td Bouma intervals. These facies are interrupted by mass-transport deposits (MTD´s) of ca. 1.5 m (Figure 2A), which indicates deposition in a near-slope environment.

In the outcrops between Metacalapa and around Pantepec we observed intercalations of thick to medium sandstone beds, 50 to 70 cm thick, with shale and thinner beds of sandstone 5 to 15 cm thick. There are cylindrical, subhorizontal, trace fossils intertwined, possibly corresponding to *Cruziana* sp. or *Megagrapton irregulare* (Figure 3E). We measured paleocurrent from flute structures at the base of the thicker sandstone beds (Figure 3D), indicating flow to the SE with little dispersion. These outcrops are interpreted as a system of wide, low sinuosity channels.

Along the rural road from Pantepec to Apipilhuaso (20.536657 ºN - 97.93102 ºW) there are excellent outcrops of a cyclic succession of fine to medium sandstone intercalated with brown laminated shale in beds 1 to 5 cm thick in outcrops that expose a laterally continuous section about 300 m thick. The section sampled at site TMI11 is about 8 m thick of fine to thin medium sandstone intercalated with brown laminated shale, interrupted by 1 m thick tabular beds of medium sandstone that present an erosive base and plane-parallel lamination (Figure 2C). At TMI11 we sampled in two closely spaced channels 1 to 1.1 m thick, which are vertically separated by splay deposits. The thickness of sandstone beds increases toward the top. The section corresponds to unconfined channels of low sinuosity and channel overbank facies. The base of sandstone bodies is abrupt but not erosional. We observed soft-sediment deformation, convolute laminations and flame structures in mudstone. The top of thick sandstone bodies is marked by layers enriched on organic matter and plant material. At site TMI9 we recognized limestone and chert lithic fragments as well as glauconite. Lithofacies at sites TMI9 to TMI11 are interpreted as unconfined channels that are interbedded channel overbank facies. Based on lithofacies and ichnofacies, we conclude that outcrops of the Chicontepec Formation near Pantepec correspond to thin bedded turbidites with the presence of channel margin facies with small channel overflow intervals, as well as wide low sinuosity and shallow channels. The thin-layered facies dominated by shale are affected by massive MTDs whose axes indicate a possible flow direction from NW to SE.

To the north, and near the town of Chicontepec (20.947814 ºN, 98.180153 ºW; site TMI15) the section is also characterized by cyclic intercalations of very fine sandstone with ripple marks and laminated shale 2 to 5 cm thick that are overlain by medium to coarse sandstone beds about 30 cm thick intercalated with thin shale intervals. This corresponds to channel overbank facies overlain by inter-channel facies. The channel-fill facies of sites TMI13 and 14 (20.818562 ºN - 98.09556 ºW; Figure 2B) are represented by a thickening and coarsening-upward succession of cyclic shales and sandstone intercalations 5 to 10 cm thick interrupted by lenticular bodies about 35 cm thick of medium-grained sandstone with planar and convolute laminations. Channels become thicker at the top of the section, reaching 1.4 m. The section is interpreted as sand-rich channels cutting into channel overbank facies. The Chicontepec Formation is affected by NW trending NE verging folds that near the mountain front may be overturned, but elsewhere are upright open folds. A NE verging thrust fault was observed near Pantepec. We estimated an average NE55 shortening direction.

3. Methodology

For the identification of magnetic mineralogy, we acquired IRM (isothermal remanent magnetization) curves, up to 3.5 T, using a pulse magnetizer. Magnetization was measured in a JR6 AGICO

http://dx.doi.org/10.18268/BSGM2022v74n1a161021

spinner magnetometer (Brno, Czech Republic). The IRM curves were modeled according to the method of Kruiver *et al.* (2001), separating IRM components of different coercivity. Since different minerals in a rock may carry a different magnetic fabric, we determined the anisotropy of magnetic susceptibility (AMS) and anisotropy of anhysteretic remanence (AARM). For the AMS we used the 15 positions protocol of the KLY-3 Kappabridge (AGICO, Brno Czech Republic), which uses an induction of 300 A/m at a frequency of 875 Hz. These results were analyzed with the software Anisoft 5.0 provided by AGICO, which determines principal susceptibility axes directions and anisotropy parameters according to Jelinek (1978).

The temperature dependence of magnetic susceptibility is used to determine the importance of the paramagnetic contribution, according to the Curie-Weiss law. AMS is the result of contributions from paramagnetic and ferromagnetic (*sensu lato*) mineral phases, assuming the diamagnetic contribution is negligible (Rochette *et al.*, 1992; Tarling and Hrouda, 1993; Borradaile and Henry, 1997; Borradaile and Jackson, 2004, 2010; Biedermann *et al.*, 2014, 2016). We measured magnetic susceptibility at low temperatures (77 to ~ 270 ºK), immersing samples in liquid nitrogen until they reached equilibrium, and we determined the magnetic susceptibility continuously as the samples warmed-up, while monitoring temperature using a thermocouple (Termómetro Omega G6). Ideal ferromagnetic behavior is constant, whilst paramagnetic behavior follows the Curie-Weiss law. When the latter was the case, we estimated the ferromagnetic contribution following Richter and Van der Pluijm (1994). These calculations exclude the range of temperatures that record magnetic transitions (e. g., Verwey). The ferromagnetic contribution is determined assuming a linear behavior of the sum of contributions from para- and ferromagnetic phases, varying the ferromagnetic contribution percentage until the correlation coefficient of a linear regression over the curve of 1/k vs. T is maximized (Richter and Van der Pluijm, 1994).

We measured the anisotropy of anhysteretic remanence following Jackson (1991). Samples were magnetized in 12 antipodal directions applying an alternating field of 80 mT and a DC field of 600 µT. Magnetizations were measured in a JR-6 spinner magnetometer and then demagnetized with inductions of 100 mT. The AARM tensor was calculated using the method of Girdler (1961) using the Rema6W software of AGICO, and the data are visualized using Anisoft 5.0 software.

4. Results

4.1. ROCK MAGNETISM

IRM acquisition curves are characterized by a steep initial ascent at low inductions. The samples are close to saturation at 0.3 T, but they do not reach saturation at 3.5 T (Figure 4). This behavior is characteristic of magnetite dominated samples with a contribution from a high coercivity phase such as hematite. The samples analyzed can be modeled (Kruiver *et al.*, 2001) with two components. A contribution from a high coercivity phase varies between 4 and 12%, with coercivities between ~ 200 and 1000 mT. The dominant low coercivity component has coercivities around 40 mT, which are characteristic of magnetite or titanomagnetite.

Figure 5 shows the susceptibility (1/k) as a function of temperature. All the samples are characterized by a ratio k_{lt}/k_{rt} greater than 3.8, which indicates the dominant contribution from paramagnetic phases (Cifelli *et al.*, 2011). The samples are characterized by a small concave inflection between ~ 100 and 120 ºK which is associated with a subdued Verwey transition. The behavior at higher temperatures is lineal following the Curie-Weiss law. This indicates a mixture of ferromagnetic (*sensu lato*) and paramagnetic behavior. The slope of the linear regression (the Curie constant) roughly corresponds to the theoretical value of biotite (Biedermann *et al.*, 2014). We note that the percentage of the contribution from ferromagnetic phases (Richter and Van der Pluijm, 1994) is

http://dx.doi.org/10.18268/BSGM2022v74n1a161021

generally smaller than ~ 30%. The paramagnetic Curie temperature is about 30 to 50 °K. Thus, collectively, phyllosilicates are the main contributors to magnetic susceptibility.

4.2. ANISOTROPY OF MAGNETIC SUSCEPTIBILITY

The bulk susceptibility of all samples is quite low, in the order of 75 x 10^{-6} SI (the range is 3.2 to 12.2 x 10^{-5} SI), which indicates that contributions from magnetite to the susceptibility are small (Rochette *et al.*, 1992). The degree of anisotropy is generally small, with Pj ranging between ~1.009 and 1.036 (Table 1), but fabrics are relatively well defined. At all sites the degree of anisotropy is independent of the bulk susceptibility. The magnetic susceptibility fabrics are not uniform. Type 1 fabrics, with k_{min} nearly perpendicular to bedding and dispersed k_{max} -k_{int} axes near the bedding plane (Robion *et al.*, 2007), were observed in sites TMI1, 9, 11, 13 and 15 (Figure 6). The fabric at these sites is oblate (Table 1). The shape of the susceptibility ellipsoid was characterized by the shape parameter T (Table 1; T < 0 = prolate; T > 0 = oblate). The magnetic foliation planes, defined by k_{max} and k_{int}, are imbricated in a direction consistent with paleocurrent directions derived from flute casts, but at TMI13 paleocurrent indicators were not available. This has been observed in flysch-type sediments (oblique magnetic foliation; Aubourg *et al.*, 2004) and it is associated with particle flow. Sites TMI9 and 11 (characterized by Bouma a-d intervals) display similar fabrics and both channels at TMI11 have similar behavior, but this contrasts with TMI10. We noticed that TMI10 is characterized by bedding-parallel laminations (upper flow regime).

Incipient tectonic fabrics (type 2; Robion *et al.*, 2007) were observed in sites TMI7, 12, and 16 (Figure 6). The fabric in sites TMI7 and TMI16 is still characterized by k_{min} near perpendicular to bedding and magnetic foliation imbricated in the upstream direction, but in contrast to type 1 fabrics, k_{max} and k_{int} are well grouped. In site TMI7 k_{max} is perpendicular to the shortening direction, but in site TMI16 k_{max} is close to the shortening direction. Imbrication is still consistent with NW to SE current flow, with small deviation. At site TMI12 a similar behavior was observed but the imbrication angle is high (~ 30°). The magnetic fabric is oblate in the group of sites that preserve sedimentary or weak tectonic fabrics, except at sites TMI9 and 13 where it is weakly prolate. The degree of anisotropy in sites with type 2 fabrics is slightly higher than in sites with type 1 fabric.

Type 3 fabrics (Robion *et al.*, 2007), with clustered k_{max} axes perpendicular to shortening and girdle distribution of k_{min} axes, were observed in sites TMI2, 3, 6, 8 and 10. Their observation in sites TMI2 and 3 is probably not due to tectonic

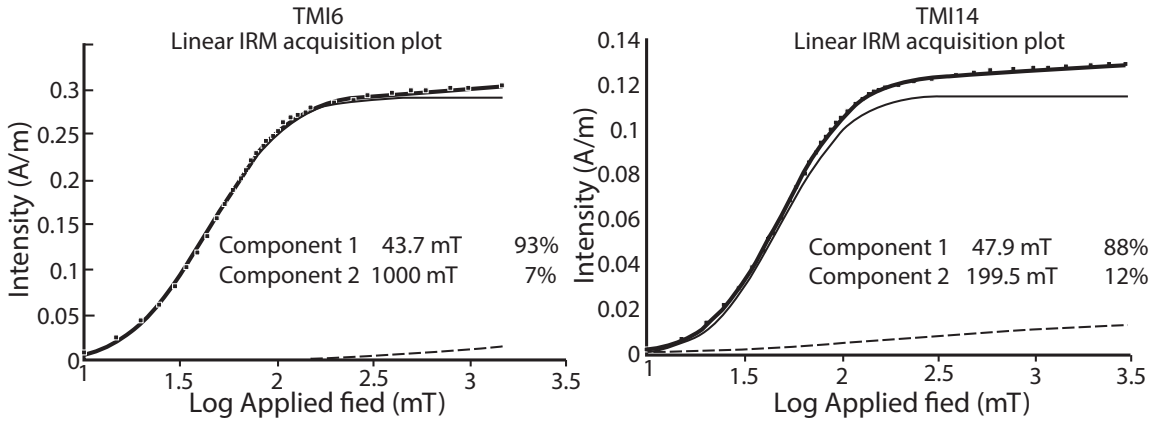

Figure 4 IRM acquisition curves of selected samples modeled with a dominant low coercivity component and a subordinate high coercivity component.

http://dx.doi.org/10.18268/BSGM2022v74n1a161021

origin since these are Oligocene and Miocene sediments that do not record significant compressional deformation. Their origin is probably hydrodynamic. The k_{max} mean axis at TMI2 closely corresponds to that observed in the nearby site TMI1 and is consistent with currents flowing to, or along the N-S or NE-SW axis that may orient elongated grains, but the lineation being an axis does not constrain the flow direction (e. g., it can be to the NE or to the SW for the case of TMI2). A similar explanation may be proposed for site TMI3, with a more northerly flow direction. For sites TMI6 and 10, k_{max} is perpendicular to the shortening direction, but for site TMI8 k_{min} is near perpendicular to the shortening direction and k_{max} is subvertical. Site TMI8 may be explained as an inverse fabric due to the presence of SD domain magnetite particles (Rochette *et al.*, 1992). Scattering of k_{min} axes towards the bedding plane (horizontal in Figure 6) reflects the loss of the sedimentary signature in sites TMI6 and 10 (Robion *et al.*, 2007); these authors favor the interpretation that type 3 fabric developed from competition between normal-to-bedding and parallel-to-bedding magnetic foliations. The large dispersion at TMI10 (possibly reflecting this competition), the orientation of k_{max} parallel to paleoflow direction, and the observation of upper-flow regime sedimentary structures suggest to us that the fabric is not tectonic, but caused instead by hydrodynamic forces.

Two sites exhibit type 4 fabrics (Robion *et al.*, 2007), with well clustered k_{max}, k_{int} and k_{min} axes. The k_{max} axis is perpendicular to the shortening direction and the k_{min} axis is nearly parallel to it (sites TMI4 and TMI5; Figure 6). Both sites correspond to thin bedded sandstone overbank facies, and shales are fissile (Figure 3B). Fabrics in these sites are oblate. These sites are from a relatively deep structural level according to field relationships. Site TMI14 displays type 5 fabrics with k_{min} horizontal and slightly deviated from shortening direction, oblate fabric, and the maximum and intermediate direction dispersed in plane near perpendicular to shortening (Robion *et al.*, 2007). The anisotropy ellipsoid of site TMI14 is markedly oblate (T = 0.754), but the sample has small degree of anisotropy (Table 1). In weakly deformed rocks type 5 tectonic fabrics may be associated with the development of cleavage, but cleavage is not present at this site.

4.3. ANISOTROPY OF ANHYSTERETIC REMANENCE

The anisotropy of anhysteretic remanence was measured at six sites (Figure 7). The degree of anisotropy of the remanence is about 1.2 (1.124 to 1.255). Ellipsoids are oblate, except for TMI10

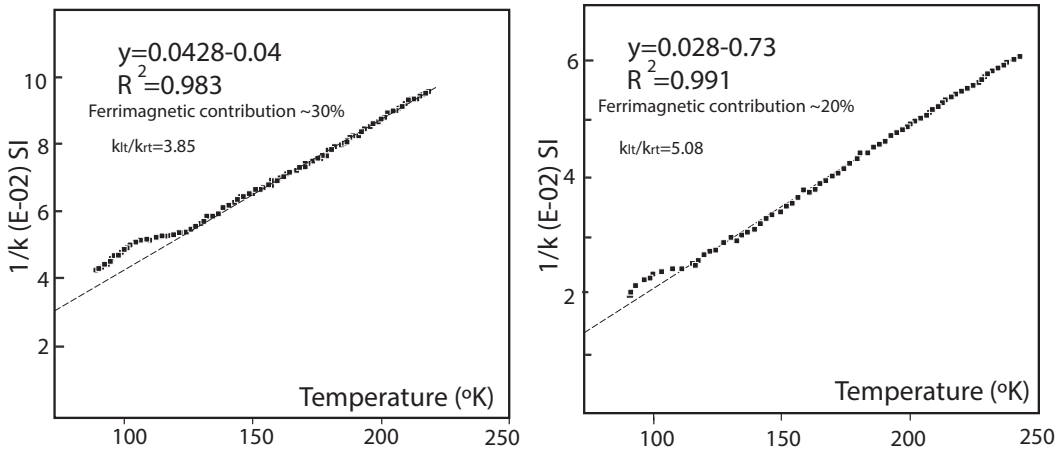

Figure 5 **Plots of the inverse value of susceptibility at low temperatures. Samples show a mixture of ferromagnetic and paramagnetic behavior, with a dominant paramagnetic contribution. The ratio k_{lt}/k_{rt} is the ratio between the susceptibility at 77 ºK and room temperature (297 ºK). The estimated ferromagnetic contribution (sensu lato) is generally smaller than ~ 30%.**

http://dx.doi.org/10.18268/BSGM2022v74n1a161021

Table 1. AMS and AARM data for Cenozoic strata in the Tampico-Misantla basin.

Site	n'/n	Lat (ºN)	Long (ºW)	Strike and dip	Kmax	Kint	Kmin	Fabric	Kmean (SI)	Pj	T	Pj AARM	T AARM
TMI1	22/24	20.57772	-97.6666	S65W/20N	214.6, 6.4	123.5, 11.5	333.6, 76.8	1	5.77 E-05	1.026	0.097	1.255	0.328
TMI2	9/12	20.59934	-97.63365	N45E/20NW	48.5,24.2	175.9,51.9	306.2,27.9	3	3.255 E-05	1.011	-0.671		
TMI3	6/8	20.43758	-97.34831	N30E/20S	342.3,20.9	84.4, 28.3	220.8,53.3	3	3.67 E-05	1.025	-0.631		
TMI4	11/11	20.52068	-97.82914	N60W/30S, N50W/30SW	316.8, 40.3	191.3,34.4	77.2,30.8	4	11.1 E-05	1.035	0.272	1.227	0.263
TMI5	6/10	20.52068	-97.82914	N60W/30S, N50W/30SW	319.4,21.4	205.4,47.2	65.4,35.8	4	10.5 E-05	1.018	0.225		
TMI6	12/15	20.491817	-97.89687	N55W/30N	149.2,13.7	41.3,51.7	249.0,35.0	3	8.27 E-05	1.017	-0.675	1.168	0.368
TMI7	8/9	20.49499	-97.89481	N35W/10S	324.9,32.4	228.8, 9.4	124.8,54.7	2	12.22 E-05	1.017	0.018		
TMI8	9/11	20.495979	-97.89888	N45W/44S	198.2,69.2	49.0,17.5	315.9,9.7	3	11.4 E-05	1.006	-0.513		
TMI9	9/13	20.520585	-97.92218	S80E/20S	276.0,21.7	6.9, 2.3	102.9,69.6	1	8.80 E-05	1.011	0.259		
TMI10	13/15	20.525473	-97.91913	N75W/20S	317.3,30.5	101.0,53.8	216.5,17.5	3	11.2 E-05	1.011	-0.312	1.167	0.004
TMI11	8/10	20.536657	-97.93102	S38W/20W	265.9,13.4	356.6, 7.7	117.7,76.1	1	8.04 E-05	1.009	0.489		
TMI12	12/13	20.80815	-97.93599	N30W/25S	262.6, 26.4	15.6,39.5	149.2,38.8	4?	5.54 E-05	1.036	0.364		
TMI13	5/8	20.818562	-98.09556	N80E/10NW	12.6,21.4	105.1, 6.4	210.8,66.5	1	6.285 E-05	1.011	0.427		
TMI14	7/8	20.818562	-98.09556	N80E/10NW	177.4,72.2	004.3,17.6	273.7,2.0	5	4.36 E-05	1.009	0.754	1.124	0.1
TMI15	12/13	20.933518	-98.19963	N85E/10N	332.1,6.3	241.1,9.0	96.5,79.0	1	7.23 E-05	1.011	0.448	1.142	0.258
TMI16	9/12	20.947814	-98.18015	N25E/10W	50.0, 6.0	318.3,16.9	160.1,72.5	2	7.98 E-05	1.012	0.508		

Here n'/n is the number of samples used/analyzed per site. Lat-Long are the latitude and longitude. Kmax, Kint and Kmin are the principal susceptibility axis. The fabric classification follows Robion *et al.* (2007). Pj are the degree of anisotropy and T the shape parameter of the ellipsoid for AMS and AARM data. Kmean is the mean bulk susceptibility.

which is neutral (T = 0.004, Table 1). In site TMI1, despite greater scatter, the AMS and AARM fabrics are roughly coaxial. The remanence degree of anisotropy is higher and the remanence ellipsoid is more oblate than in the AMS fabric. In site TMI4 the AMS and AARM ellipsoids are again roughly parallel, but the positions of the k_{max} and k_{int} are interchanged, the remanence susceptibility maximum is oriented to the SW. This indicates that elongated magnetite grains are preferentially aligned roughly parallel to the shortening direction. In both methods, the fabric is a composite type 4 fabric. At TMI6, where the AMS type 3 fabric is relatively ill defined, the AARM fabric is triaxial. All three axes are well clustered, k_{min} is roughly perpendicular to bedding and k_{max} is horizontal, roughly parallel to the shortening direction, but is perfectly perpendicular to the paleocurrent direction (Figure 7).

The AARM fabric at site TMI10 is also better defined than the AMS fabric, but the position of k_{min} in the AMS corresponds to the position of maximum susceptibility of remanence, the position of k_{max} corresponds to the intermediate remanence, and the remanence susceptibility minimum is oriented at a shallow angle to the SE (similar to TMI4). In TMI10 and TMI4 the migration of the minimum axis towards the horizontal appears to indicate a fabric of tectonic origin. Site TMI14, which records a type 5 AMS tectonic fabric records a similar type 5 AARM fabric. The coherence of AARM and AMS fabrics at TMI14 supports its interpretation as a tectonic fabric, but we find no convincing interpretation for the presence of tectonic fabric in this site nor for the preservation of sedimentary fabric at TMI13. This site preserves graded bedding, bedding parallel laminations and convolute laminations; the plastic and ductile conditions necessary for the formation of convolutions during deposition are provided by sets of muddy and silty lamina (Sanders, 1960). Cohesive forces and early cementation may be the same forces that

http://dx.doi.org/10.18268/BSGM2022v74n1a161021

preserved a sedimentary fabric at TMI13. Finally, site TMI15, which records a type 2 AMS fabric, records a strongly oblate fabric with relatively well clustered minimum remanence susceptibility to the NW and shallow. This seems to correspond to an inverse fabric where the (inverse) lineation indicates the paleo flow direction.

In the Jelinek diagram (Jelinek, 1981) there is an apparent development of fabric in response to progressive deformation from sites in the oblate field with weak low degree of anisotropy (e. g., sites TMI9, 11, 13 and 15; Figure 8), to prolate sites with weak tectonic fabric (TMI6 and 10), to sites with more developed tectonic fabric (TMI4 and 5). There are, however, sites that depart from the expected trend, such as TMI12 and TMI14. Both AARM and AMS indicate that TMI14 has a well-developed type 5 tectonic fabric, but the site does not plot in the expected area of the diagram. Site TMI12 also seems to be anomalous. We suggest that rather than a high imbrication angle in a sedimentary fabric, this site must be interpreted as a tectonic, approaching a type 4 fabric, with migration of k_{min} toward the bedding plane.

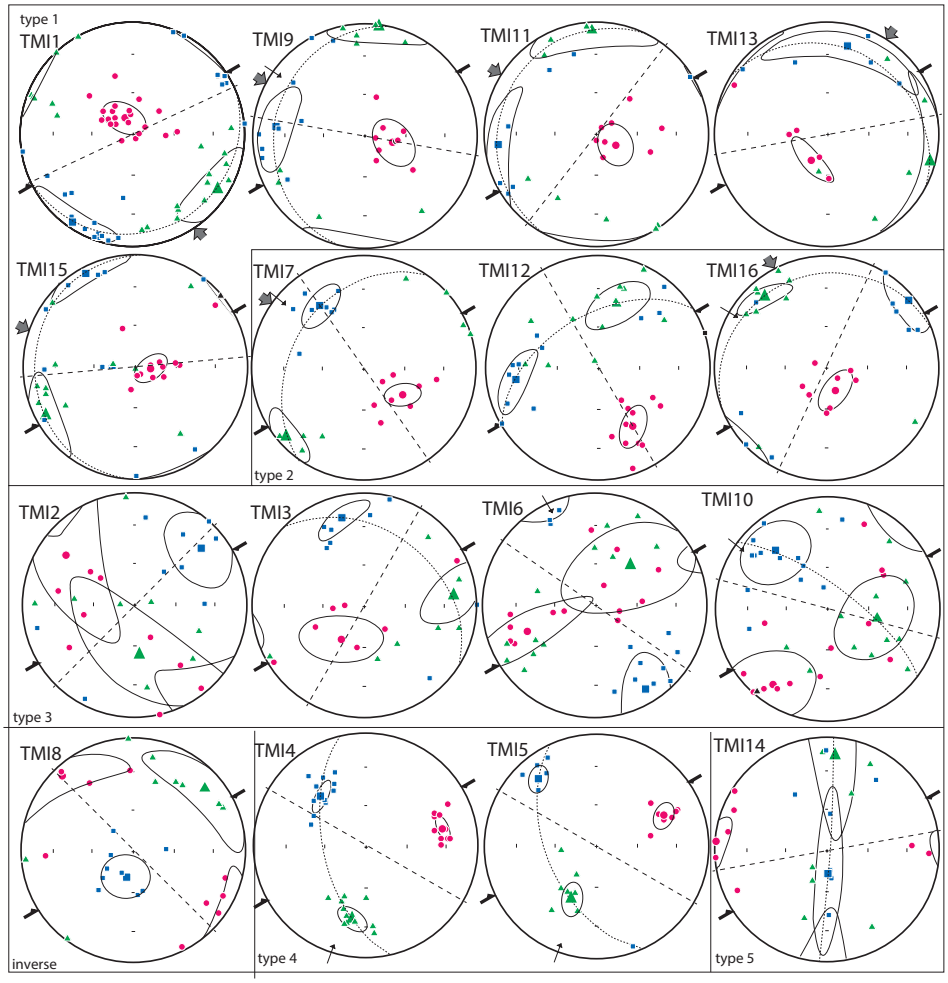

Figure 6 Anisotropy of magnetic susceptibility results in equal area lower hemisphere stereographic projections. Maximum, intermediate and minimum susceptibility directions correspond to squares, triangles and circles, respectively. Thick arrows indicate shortening direction and thin arrows are paleocurrent directions derived from flute-cast orientation. The magnetic foliation is marked with a dotted line and a dashed line indicates the strike of bedding. A dashed arrow indicated inferred flow direction from magnetic fabric. Directions are plotted restored to the paleohorizontal.

http://dx.doi.org/10.18268/BSGM2022v74n1a161021

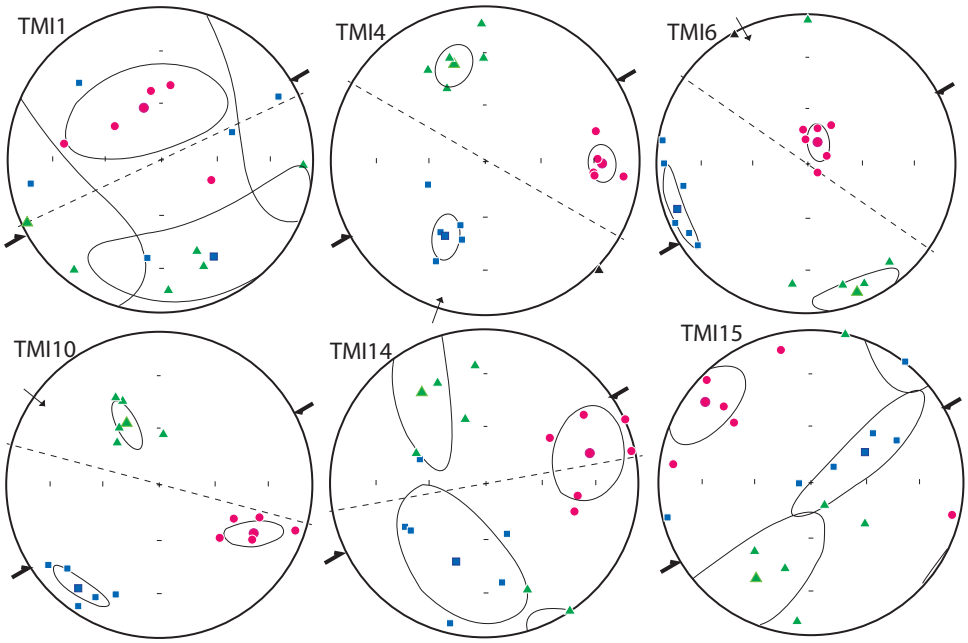

Figure 7 Anisotropy of anhysteretic remanence (AARM) of selected sites. Symbols as in Figure 6.

5. Discussion

The rock magnetic experiments, albeit limited, produce relatively straightforward conclusions. The main ferromagnetic phase is a cubic phase, and the coercivity is consistent with this phase being magnetite (Day *et al.*, 1976). This observation applies to all the sampled sites, where the contribution from this phase to the IRM acquisition curve is ~ 90%. There is a small contribution from a high coercivity phase. The coercivity is consistent with values observed in hematite. The low temperature measurements indicate that the contributions from paramagnetic phases to the bulk susceptibility are generally greater than ~ 70%. The Curie constant is consistent with phyllosilicates being the main minerals that contribute to the paramagnetic susceptibility, and their platy morphology makes them susceptible to orientation by the action of currents.

Sedimentary structures and facies associations are consistent with sampling of sandstone rich channels and thin bedded turbidites, with the presence of channel margin facies with small channel overbank intervals. Channel-fill facies correspond to wide low sinuosity channels. Preservation of plane laminations in sandstones and current ripple laminations in turbidity deposits (Boumma b, c, and d) indicate variable fluid flow conditions, thus grains may be aligned by strong currents of flow in topset laminations at sites such as TMI1, 7, 9, 11, 12, 13, 15 and 16. Grain alignment is also developed during upper flow regimes (sites TMI6 and 10).

The paleocurrent indicators in sites collected at one locality in the Palma Real Formation indicate paleo-flow from the south or SW. Paleocurrent indicators (mostly flute casts) in the Chicontepec Formation indicate mostly flow from the NW. The AMS fabric reproduces these current indicators by either imbrication of the magnetic foliation plane, for example in sites TMI1, TMI9 and TMI11; paleo-flow direction is also associated with magnetic lineation at some sites (TMI2 and TMI3). In sites TMI7 and 16 a NW to SE flow is also interpreted from imbrication of the magnetic foliation plane, even if the fabric is not fully sedimentary. Most other sites, however, record composite or incipient tectonic fabrics consistent with NE

http://dx.doi.org/10.18268/BSGM2022v74n1a161021

directed compressional stress developing type 4 and type 5 fabrics. The coincidence of paleo-flow direction with the general direction of the fold axis makes this inference ambiguous, but the migration of k_{min} towards the bedding plane supports a tectonic origin for the type 3 fabric in sites such as TMI6 and TMI10. For site TMI8 we favor the interpretation of an inverse fabric, but we lack the experimental data to support such interpretation. For site TMI8 as well as site TMI13 interpreted flow directions are from the N or NNE; these directions do not follow the general NW trend observed in the Chicontepec Formation, but they may reflect local variations due to the shelf-slope morphology.

Anisotropy of ARM sheds additional information to these interpretations but the results are not straightforward. Site TMI1 requires little discussion because the fabrics of AMS and AARM are coaxial. We therefore discuss site TMI4, as a site with a well developed type 4 fabric; AMS and AARM are coaxial, with similar k_{min} directions, but interchanged intermediate and maximum direction. A plausible interpretation is that in this sample there is a sum of two fabrics. A dominant fabric is caused by the paramagnetic phases. Deformation tends to align the phyllosilicate minerals in the direction of incipient planar axial cleavage (NW-SE) with a NW directed lineation, but the ferromagnetic fabric is caused by the preferential alignment of elongated magnetite grains in the direction of thrust movement as reported by Pueyo *et al.* (2010). When added, these results in intermediate and maximum susceptibility directions streaked along the AMS foliation plane. A similar explanation may be proposed for site TMI10, but at this site the AMS fabric is strongly prolate, with k_{max} perpendicular direction to the shortening direction. This fabric may result from an inherited sedimentary fabric. For the AARM the maximum axis is to the SW parallel to the direction of thrust motion. Thrusting was recognized at this locality near Pantepec.

Site TMI6 is more puzzling. The AMS fabric is prolate and this site preserves a type 3 fabric with NW directed lineation (k_{max}). The other two axes are scattered in a plane parallel to the shortening direction. The AARM fabric is type 2, a sedimentary fabric weakly modified by deformation. The minimum remanence axis is near perpendicular to bedding at a steep ENE directed angle. We note that there is a cluster of k_{min} directions in the AMS data in the same general direction. Because of the presence of layer parallel laminations (upper flow

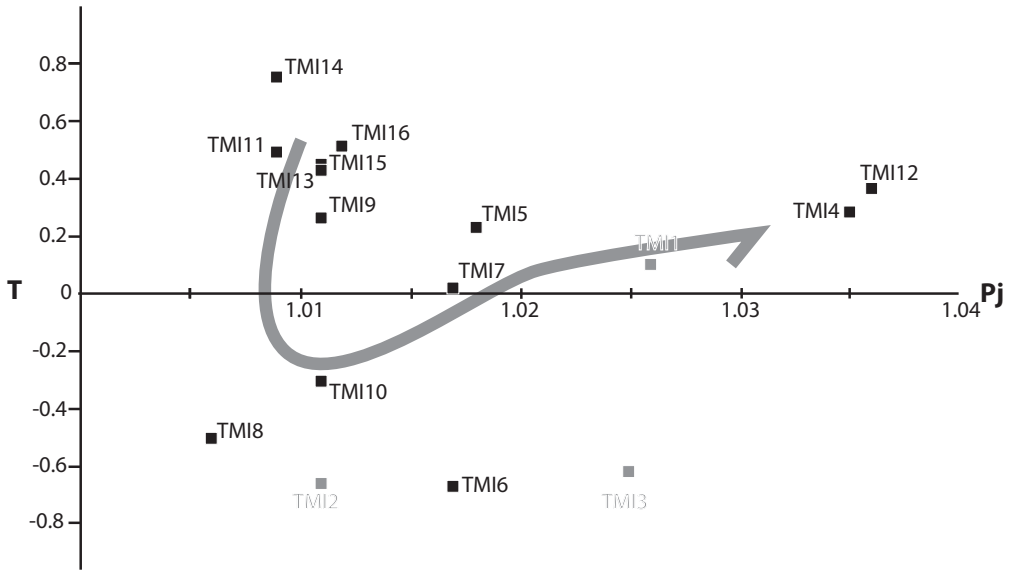

Figure 8 Jelinek diagram (Jelinek, 1981) showing partial development of tectonic fabric as a response to progressive deformation.

http://dx.doi.org/10.18268/BSGM2022v74n1a161021

regime) the fabric of TMI6 appears to be related to alignment of elongated magnetite particles rolling perpendicular to the flow direction (they provide the orientation of the maximum remanence axis) but the paramagnetic fraction more susceptible to reorientation is aligned with k_{max} parallel to the fold axis (normal to shortening).

For site TMI14, which records a type 5 fabric (the most developed tectonic fabric) the AARM and AMS are close to coaxial, but the minimum remanence direction does not reach the horizontal. This seems to indicate the lower efficiency of the deformation process to realign the more rigid ferrimagnetic particles. Finally, for site TMI15 a simple explanation is not easy to obtain. The AMS fabric is sedimentary and consistent with paleo-flow direction from the NW. The AARM fabric is oblate with a k_{min} directed to the NW near horizontal. A possible explanation could be the presence of an inverse fabric recorded by AARM, but it is not reflected in the AMS measurements. This explanation is supported by the absence of a Verwey transition and a very small (< 10%) contribution from ferromagnetic susceptibility.

6. Conclusions

The rock magnetic data indicate that magnetite is the dominant ferrimagnetic phase, but the AMS is dominated by paramagnetic minerals (biotite and other phyllosilicates). The magnetic anisotropy of remanence and susceptibility record different hydrodynamic processes at some sites, and the response to deformation is not the same possibly because of the low intensity of deformation. The AMS fabric reproduces with relatively good fidelity paleo-flow direction, confirming the NW to SE dispersion of sediment in the Chicontepec paleo-canyon, but with some dispersion since NNE to SSW flowing channels were also recognized. In contrast, sediments in Oligocene and younger units, with a very limited data set, appear to have been derived from southern sources. AMS and AARM fabrics may combine in complex patterns. AARM appears to record either maximum axis directions that correspond to alignment of elongated particles perpendicular to flow or, more likely, record the direction of thrust motion. This study indicates that magnetic fabric can be used as a good approximation of paleocurrent directions in the Chicontepec canyon system.

Author contributions

R.S. Molina Garza: Experimental design, field work, interpretations of magnetic fabric data, manuscript preparation. M.I. Sierra Rojas: Field work, sedimentological observations and interpretations, manuscript preparation.

Financing

We thank CONACYT program Proyectos de Investigación en Fronteras de la Ciencia 2016 -1787, for financial support.

Acknowledgements

We also thank Leidy J. Ortiz and Cristian Valbuena for assistance in the field and in the laboratory. We thank Xochitl Torres and an anonymous reviewer for their comments on the original version of this manuscript.

Conflict of interest

Authors declare that there are no conflicts of interest in developing this research.

References

Aubourg, C., Smith, B., Bakhtari, H., Guya, N., Eshragi, A., Lallemant, S., Molinaro, M., Braud, X., Delaunay, S., 2004, Post-Miocene shortening pictured by magnetic fabric across the Zagros–Makran syntaxis (Iran), in Sussman, A. J., Weil, A. B. (Eds.), Orogenic

http://dx.doi.org/10.18268/BSGM2022v74n1a161021

Curvature: Integrating Paleomagnetic and Structural Analysis: Boulder, Colorado, Geological Society of America Special Paper, 383, 17–40. https://doi.org/10.1130/0-8137-2383-3(2004)383[17:pspbmf]2.0.co;2

Biedermann, A. R., Koch, C. B., Lorenz, W. E., Hirt, A. M., 2014, Low-temperature magnetic anisotropy in micas and chlorite: Tectonophysics, 629, 63-74. https://doi.org/10.1016/j.tecto.2014.01.015

Biedermann, A. R., Pettke, T., Angel, R. J., Hirt, A.M., 2016, Anisotropy of magnetic susceptibility in alkali feldspar and plagioclase: Geophysical Supplements to the Monthly Notices of the Royal Astronomical Society, 205(1), 479-489. https://doi.org/10.1093/gji/ggw042

Borradaile, G. J., 1988, Magnetic susceptibility, petrofabric and strain: Tectonophysics, 156, 1-20. https://doi.org/10.1016/0040-1951(88)90279-x

Borradaile, G. J., Fralick, P.W., Lagroix, F., 1999, Acquisition of anhysteretic remanence and tensor substraction from AMS isolates true paleocurrent grain alignements, in Tarling, D. H., Turner, P. (Eds.), Paleomagnetism and Diagenesis in Sediments: Geological Society, London, Special Publications,151. 139–145. https://doi.org/10.1144/gsl.sp.1999.151.01.14

Borradaile, G. J., Henry, B., 1997, Tectonic applications of magnetic susceptibility and its anisotropy: Earth Science Reviews 42, 49–93. https://doi.org/10.1016/s0012-8252(96)00044-x

Borradaile, G. J., and Jackson, M., 2004, Anisotropy of magnetic susceptibility (AMS): magnetic petrofabrics of deformed rocks: Geological Society, London, Special Publications, 238(1), 299-360. https://doi.org/10.1144/gsl.sp.2004.238.01.18

Borradaile, G. J., Jackson, M., 2010, Structural geology, petrofabrics and magnetic fabrics (AMS, AARM, AIRM): Journal of Structural Geology, 32(10), 1519-1551. https://doi.org/10.1016/j.jsg.2009.09.006

Busch, D. A., Amado, G. S., 1978, Stratigraphy and structure of Chicontepec turbidites, southeastern Tampico Misantla basin, Mexico: American Association of Petroleum Geologists Bulletin, 62, 235-246. https://doi.org/10.1306/c1ea481f-16c9-11d7-8645000102c1865d

Cifelli, F., Minelli, L., Rossetti, F., Urru, G., Mattei, M., 2012, The emplacement of the Late Miocene Monte Capanne intrusion (Elba Island, Central Italy): constraints from magnetic fabric analyses: International Journal of Earth Sciences, 101(3), 787-802. https://doi.org/10.1007/s00531-011-0701-z

Cossey, S. P. J., Bitter, M. R., Dickens, G. R., Van Nieuwenhuise, D., Pindell, J., Rosenfeld, J. H., Beltrán-Treviño, Cornick, P., Agnini, C., 2019, Paleo-canyon formation and contemporaneous oil seepage near the Paleocene/Eocene boundary, Tampico-Misantla basin, eastern Mexico: GeoGulf Transactions, 69, 27-53.

González-Díaz, M. G., Lawton, T., Juárez-Arriaga, E., Fitz-Diaz, E., Solari, L., 2018, Análisis estratigráfico de la Formación Chicontepec en el Norte de la Cuenca Tampico-Misantla, México: La Sierra Madre Oriental como una fuente de sedimentos: Geos, 38 (1), 204.

Girdler, R. W., 1961, The measurement and computation of anisotropy of magnetic susceptibility in rocks: Geophysical Journal International, 5, 34– 44. https://doi.org/10.1111/j.1365-246x.1961.tb02927.x

Graham, J. W., 1966, Significance of magnetic anisotropy in Appalachian sedimentary rocks, in Steinhart, J. S. and Smith, T. J. (eds.), The Earth Beneath the Continents: Geophysical Monograph Series, 10, 627-648.https://doi.org/10.1029/gm010p0627

Hamilton, N., Rees, A. F., 1970, The use of anisotropy of magnetic fabric in palaeocurrent estimation, in Runcorn, S. K. (ed.) Palaeogeophysics, Oxford, 445-463.

Hrouda, F., 1982, Magnetic anisotropy of

rocks and its applications in geology and geophysics: Geophysical Surveys, 5, 37-81. https://doi.org/10.1007/bf01450244

Imaz, A. G., Pocoví, A., Lago, M., Parés, J. M., 2000, Effect of lithostatic pressure and tectonic deformation on the magnetic fabric (anisotropy of magnetic susceptibility) in low-grade metamorphic rocks: Journal of Geophysical Research 105 (B9), 21, 305. (2000JB900171). https://doi.org/10.1029/2000jb900171

Jackson, M. J., 1991, Anisotropy of magnetic remanence: A brief review of mineralogical sources, physical origins, and geological applications, and comparison with susceptibility anisotropy: Pure and Applied Geophysics, 136, 1 –28. https://doi.org/10.1007/bf00878885

Jelinek, V., 1978, Statistical processing of anisotropy of magnetic susceptibility measured on groups of specimen: Studia Geophysica et Geodaetica. 22, 50–62. https://doi.org/10.1007/bf01613632

Jelinek, V., 1981, Characterization of the magnetic fabrics of rocks: Tectonophysics, 79, T63-T67. doi.org/10.1016/0040-1951(81)90110-4

Kruiver, P. P., Dekkers, M. J., Heslop, D., 2001, Quantification of magnetic coercivity components by the analysis of acquisition curves of isothermal remanent magnetization: Earth and Planetary Science Letters, 189(3-4), 269-276. https://doi.org/10.1016/s0012-821x(01)00367-3

Parés, J. M., van der Pluijm, B. A, Dinarés-Turell, J., 1999, Evolution of magnetic fabrics during incipient deformation of mudrocks (Pyrenees, northern Spain): Tectonophysics, 307, 1-14. https://doi.org/10.1016/s0040-1951(99)00115-8

Pueyo Anchuela, O., Imaz, A. G., Pocoví, J. A, 2010, Significance of AMS in multilayered systems in fold-and-thrust belts. A case study from the Eocene turbidites in the southern Pyrenees (Spain): Geological Journal, 45, 544-561. doi.org/10.1002/gj.1194

Rees, A. I., Woodal, W. A., 1975, The magnetic fabric of some laboratory-deposited sediments: Earth and Planetary Science Letters, 25, 121-130. https://doi.org/10.1016/0012-821x(75)90188-0

Richter, C., and van der Pluijm, B. A., 1994, Separation of paramagnetic and ferrimagnetic susceptibilities using low temperature magnetic susceptibilities and comparison with high field methods: Physics of the Earth and Planetary Interiors, 82(2), 113-123. https://doi.org/10.1016/0031-9201(94)90084-1

Robion, P., Grelaud, S., Frizon de Lamotte, D., 2007, Pre-folding magnetic fabrics in fold-and-thrust belts: Why the apparent internal deformation of the sedimentary rocks from the Minervois basin (NE Pyrenees, France), is so high compared to the Potwar basin (SW Himalaya, Pakistan)?: Sedimentary Geology, 196, 181-200. https://doi.org/10.1016/j.sedgeo.2006.08.007

Rochette, P., Jackson, M., Aubourg, C., 1992, Rock magnetism and the interpretation of anisotropy of magnetic susceptibility: Reviews of Geophysics, 30(3), 209-226. https://doi.org/10.1029/92rg00733

Sanders, J. E., 1960, Origin of convoluted laminae: Geological Magazine, 97, 409-421.

Santillán-Piña, N., Aguayo-Camargo, J. E., 2011, Facies sedimentarias turbidíticas del Terciario Inferior en la Cuenca de Chicontepec, Centro-Oriente de México: Ingeniería Investigación y Tecnología, 12-3, 337-352.

Servicio Geológico Mexicano, 2004, Carta Geológico-Minera Poza Rica. Scale 1:250,000. Pachuca, Mexico.

Tarling, D., Hrouda, F. (Eds.), 1993, Magnetic anisotropy of rocks. Chapman & Hall, 217. https://doi.org/10.1002/gj.3350300111